AD-A045 385 NORTHWESTERN UNIV EVANSTON ILL DEPT OF MECHANICAL E--ETC F/G 11/6
LEAD MICROCLUSTERS IN THE VAPOR PHASE AS STUDIED BY MOLECULAR B--ETC(U)
SEP 77 A YOKOZEKI N00014-76-C-0378
UNCLASSIFIED TR-4 NL

| OF |
AD
A045385

END
DATE FILMED
11-77
DDC

SECURITY CLASSIFICATION OF THIS PAGE (When Data Entered)

REPORT DOCUMENTATION PAGE

READ INSTRUCTIONS BEFORE COMPLETING FORM

1. REPORT NUMBER: N00014-76-C-0378-TR4
2. GOVT ACCESSION NO.:
3. RECIPIENT'S CATALOG NUMBER:

4. TITLE (and Subtitle): LEAD MICROCLUSTERS IN THE VAPOR PHASE AS STUDIED BY MOLECULAR BEAM-ELECTRON DIFFRACTION: VESTIGE OF AMORPHOUS STRUCTURE

5. TYPE OF REPORT & PERIOD COVERED: Technical Report

6. PERFORMING ORG. REPORT NUMBER: TR-4

7. AUTHOR(s): Akimichi Yokozeki

8. CONTRACT OR GRANT NUMBER(s): N00014-76-C-0378

9. PERFORMING ORGANIZATION NAME AND ADDRESS:
Northwestern University
Dept. of Mechanical Engineering and
Astronautical Sciences - Evanston, IL 60201

10. PROGRAM ELEMENT, PROJECT, TASK AREA & WORK UNIT NUMBERS: NR092-544

11. CONTROLLING OFFICE NAME AND ADDRESS:
Office of Naval Research
Arlington, VA 22217

12. REPORT DATE: Sept[illegible] 1977

13. NUMBER OF PAGES: ~~33~~ 12 34p.

14. MONITORING AGENCY NAME & ADDRESS (if different from Controlling Office):
ONR, Chicago
536 S. Clark Street
Chicago, IL 60605

15. SECURITY CLASS. (of this report): Unclassified

15a. DECLASSIFICATION/DOWNGRADING SCHEDULE:

16. DISTRIBUTION STATEMENT (of this Report)

Distribution of this document is unlimited.

17. DISTRIBUTION STATEMENT (of the abstract entered in Block 20, if different from Report)

18. SUPPLEMENTARY NOTES

19. KEY WORDS (Continue on reverse side if necessary and identify by block number)

Microcrystals, Clusters, Nucleation, Molecular Beam, Electron Diffraction

20. ABSTRACT (Continue on reverse side if necessary and identify by block number)

The metal microclusters are formed in the gas phase by an isobaric cooling due to argon carrier gas, followed by adiabatic expansions through nozzle apertures. Electron diffraction patterns of these condensates show the typical Debye-Scherrer rings for the f.c.c. Pb metal. The average size of clusters obtained, depending on the experimental conditions, ranges from 30 to 100 Å in diameter, and the cubic lattice parameters for these clusters are essentially the same, within an experimental error of 0.3%, as that for →over

DD FORM 1 JAN 73 1473 EDITION OF 1 NOV 65 IS OBSOLETE
S/N 0102-014-6601

SECURITY CLASSIFICATION OF THIS PAGE (When Data Entered)

ANGSTROM

403 502

the bulk crystal. The analysis of the Bragg-peak intensities is carried out based on the usual kinematical theory and the dynamical (two-beam approximation) theory by Blackman. The former theory fails completely in accounting for small angle reflections ($s \leq 5$ Å^{-1}), whereas the latter explains successfully the whole observed intensities, except for the 2nd and 3rd order reflections (400), (440), (333) and (600). From the damping of peak intensities, the temperatures of these clusters are estimated to be of the order of 150°K.

A close inspection on the comparison between the observed and theoretical intensities, however, reveals periodic fluctuations in the observed peak heights as a function of the scattering angle, indicating a superposition of some diffuse scattering. The amplitudes of the fluctuations are more marked for the smaller size clusters. The characteristics of the fluctuations are accounted for by introducing liquid-like random atomic configurations into the microcrystalline. This model explains also the abnormal Bragg-peak intensities of Ar clusters, reported in the literature.

TABLE OF CONTENTS

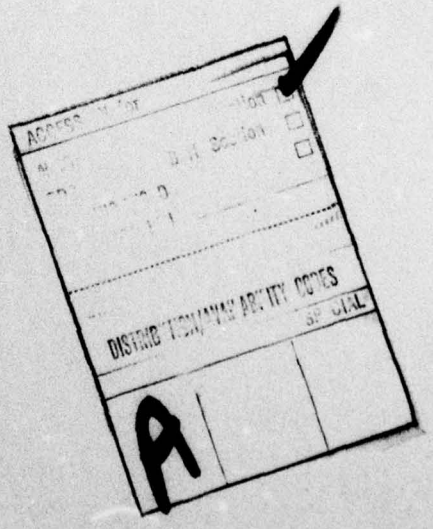

INTRODUCTION

Little has been known about the structure of microcrystals, despite extensive theoretical and experimental works. Electron diffraction observations for clusters above a certain size show the Bragg reflection peaks, characteristic of the regular lattice of bulk crystals. Does this mean that such a cluster is simply a micro-replica of bulk materials? The question could be answered by a detailed analysis of the reflection intensity, instead of the simple lattice parameter analysis. Farges et al.[1] observed the anomaly in some of the reflection intensities of Ar clusters consisting of 500~1000 atoms, suggesting an amorphous nature of the microcrystal structure. For very small sizes of clusters (say, $<$ 500 atoms), diffraction patterns become similar to those in bulk liquid, as observed in Ar clusters.[2,3] According to theoretical model calculations,[4-6] the structure of microclusters is different in quality from the bulk lattice structure and even amorphous for small sizes of aggregates. The structure and stability of microclusters depend strongly on the size of aggregates. Microclusters are in a pseudo-steady state and their structures evolve through a so-called critical size. Such a dynamical

aspect of the cluster structure is an important clue to understand phase change phenomena, nucleation kinetics, and catalytic activities of metal clusters, etc.[7)]

Thus, our immediate concern is to shed some light on such a cluster structure by means of molecular beam - electron diffraction. So far metal clusters have not been studied by this method,[8)] though thin film experiments are well known. An advantage of this technique over the thin film is that clusters can be produced by homogeneous nucleation, and their diffraction patterns are free from the sample-supporting material for films. Such supporting materials, being amorphous, give a diffuse scattering background, by which the measurement of reflection peak intensities is sometimes disturbed. A difficulty in the present method, however, is to prepare the cluster sample with desired sizes. Supersonic expansions, as successfully used for simple gas samples (Ar, CO_2, etc.),[1,2,9)] are not practical for metals. Cooling of metal vapor by a cold carrier gas produces easily metal clusters, but for the sampling of desired sizes of clusters a proper nozzle must be designed for the diffraction experiment. A simple nozzle for this purpose has been constructed to produce a metal cluster beam.[8)] This nozzle has enabled us to study the structure of lead metal clusters, for the first time, in their free state (gas phase).

Lead has been chosen for the following reasons; 1) technical ease of vaporization; 2) well-known bulk properties which are useful for the analysis; 3) a simple structure of the bulk crystal (face-centered cubic; f.c.c.), which is the same as Ar solid;—— Ar clusters are most extensively studied and standard samples for the cluster-structure study; and 4) possible importance of dynamical

(multiple scattering) effects[10] due to the heavy atoms (Z = 82), being different from the case of Ar clusters.

EXPERIMENTAL

The metal-cluster-beam nozzle used in this study is schematically shown in Fig. 1; a more detailed description of this nozzle will be reported elsewhere.[8] Lead (99.999% purity, purchased from Goldsmith Chem. & Metal Corp.) was evaporated from an electrically heated tungsten filament oven (H), and mixed with argon carrier gas at about 0.6 cm downstream from H. The ambient temperature (T_a) around this mixing region was monitored with a Chromel-Alumel thermocouple (TC), while the temperature of metal on the filament was measured by an optical pyrometer through a small back window (W). No special cooling system was required for this nozzle assembly because of a small heat capacity of the filament oven, though the filament temperature was typically 900—1000°C. Condensation of metal vapor occurs through an isobaric cooling by argon carrier gas at the mixing region, where the distance (L_h) from the heater H to the first nozzle aperture (N_1) is adjustable (1.6 — 3.6 cm). The condensates further cool by two-stage adiabatic expansions through N_1 (diam: 0.076 cm) and N_2 (diam: 0.050 cm) nozzle apertures. The pressure drop by these free jet expansions was of the order of 2×10^{-5}. The expansions form a well-collimated metal cluster beam with an angular width of about 5°; at about 50 cm downstream, a circular shape deposit (c.a. 4.5 cm in diameter) of metal was observed. In order to change an average size of metal clusters, the distance L_h, argon gas pressure (P_a) and the filament temperature (T_m) were varied. Although no attempt was made to study the nucleation kinetics,

it was found by some trial-and-error experiments that P_a and T_m were effective parameters to control the cluster size.[8)]

The metal cluster beam generated by this nozzle was crossed with an electron beam[10)] (with an accelerating voltage of 40 kV and an electron beam current of 4.6 μA) at 0.064 cm distant from the nozzle tip (N_2) in the diffraction chamber, where the ambient pressure of $(0.8 - 1.2)\times10^{-5}$ torr was maintained during the experiments. The metal beam diameter at the point to cross the electron beam was measured to be 0.056 cm from a size of a trace of metal deposit on a thin Al plate which was placed at the crossing point. This spread of beams causes only a minor correction to the line broadening of diffraction patterns. Diffraction patterns of Pb cluster beams were recorded on Kodak Electron Image plates ($3\frac{1}{4}\times4$") at a nozzle-to-plate distance (L) of 53 cm without a sector. The magnetic field from the heater current (D.C. regulated: max. 30Amp) produced on the photographic plate a deflection of less than 0.2 cm, which was compensated by moving the beam stop and/or tilting the electron gun unit mechanically. For the instrumental calibration, diffraction patterns for standard thin metal films of Al, Au and Pb were also recorded. These provided the camera constant $L\lambda$ (λ = electron wave length) and an estimate of the instrumental line broadening of Debye-Scherrer rings.

Three typical plates (denoted as A, B and C) were chosen for the following analysis. The experimental conditions are given in Table 1. The densitometric traces for these plates are shown in Fig. 2. In order to convert the photographic density (d) to the relative intensity (I), the following equation was used.[11)]

$$I = d(1+cd) \qquad (1)$$

,where $c = 0.1$ for $d \lesssim 2.0$. This equation fitted a measured density-exposure calibration curve.

ANALYSIS AND RESULTS

I) Peak Positions and Widths

According to the Bragg condition, the peak position of diffraction pattern is given by,

$$s = 2\pi / d_{hkl} \qquad (2)$$

,where $s = (4\pi/\lambda)\sin\theta$ (diffraction angle $= 2\theta$), and d_{hkl} is the inter-planar distance with the Miller indices (hkl). For a f.c.c. crystal and a small diffraction angle (in the present case, $\theta \lesssim 4.3\times10^{-2}$ radians), eq. (2) can be expressed by a radius (r) of the Debye-Scherrer ring for plane (hkl), the camera constant ($L\lambda$) and the lattice constant (a).

$$r/L\lambda \propto 1/d_{hkl} = (h^2 + k^2 + l^2)^{\frac{1}{2}}/a \qquad (3)$$

Once each ring is indexed by the standard procedure (see Fig. 2), the measurement of the ring diameter provides the lattice parameter. The systematic error due to the small angle approximation in eq. (3) can be sufficiently corrected by the use of $r - 3r^3/8L^2$ ($L = 53$ cm) instead of r. This correction becomes important for outer rings; e.g., the correction for a (531) ring results in an increase of 0.01 Å in the lattice parameter. The results are summarized in Table 2 for the three chosen plates A, B and C.

The width of Bragg peaks provides an estimate of the average cluster size, as has been used in X-ray powder patterns;[12] after correcting the instrumental broadening, which was estimated by taking diffraction patterns of standard thin films; see experimental section. The broadening due to the cluster beam spread was of negligible importance, compared to the above source. For the estimate of the average cluster size (diameter: D), well-resolved (111) and (220) peaks were used with assuming the unit shape factor;[12] and the results are given in the lower section of Table 2 for the three plates. The errors given in the Table were estimated from uncertainties in the instrumental-broadening correction and in the line-width measurement. The average size D can also be obtained independently from the following peak-intensity analysis.

II) Peak Intensity

The relative intensity of Bragg peaks was obtained by subtracting the background intensity from the experimental curves, which were calibrated by eq. (1) to the relative intensities. Smooth background curves (base line for the Bragg peaks) were drawn without ambiguity for the three plates. In order to examine systematic background errors, if any, due to the instrument, diffraction patterns of pure argon gas were taken under experimental conditions similar to those in the metal sample. No discernible systematic fluctuation or periodicity was observed. The observed peak intensities I_{obs}, being normalized to 100 at the (111) peak, are listed in Table 2.

The relative peak intensity, I_{Bragg}, may be calculated by the usual kinematical expression for X-ray powder pattern[13] with a small

angle approximation:

$$I_{Bragg} = |F_{hkl}|^2 \cdot P_{hkl} \cdot d_{hkl}^2 \cdot e^{-2M} \equiv I_{kin} \cdot e^{-2M} \qquad (4)$$

$$|F_{hkl}| = \sum_j f_j \cdot \exp[2\pi i(hx_j + ky_j + lz_j)] = 4f \qquad (5)$$

, where f_j is the elastic atomic scattering factor of electron for the j^{th} atom with a coordinate (x_j, y_j, z_j) in a unit cell. P_{hkl} is a multiplicity of the (hkl) reflection with the interplanar distance d_{hkl}. The Debye-Waller factor e^{-2M} can be expressed with an isotropic square mean amplitude $(\bar{u}^2)$ of lattice vibrations: $e^{-2M} = \exp(-\bar{u}^2 s^2)$. A plot of $\ln(I_{obs}/I_{kin})$ vs. s^2 should give a straight line with a negative slope of $\bar{u}^2$, if eq. (4) holds for the present case. However, such plots showed a marked deviation from a straight line for low angle peaks ($s \lesssim 5$ Å^{-1}) and for the 2nd order reflections (400) and (440). The observed intensities for these peaks are too weak: e.g., 80% and 50% lower than the kinematical values for the (111) and (400) peaks, respectively. This is illustrated in Fig. 3 by the curve (5) in the case of Plate A. The failure of the kinematical theory in electron diffraction is to be expected for a microcrystal, specially one which consists of heavy atoms such as Pb (Z = 82), since the attenuation (or extinction) of the original electron wave due to interatomic multiple scatterings (or dynamical interaction effects) is more important than that of X-ray, because of the stronger interaction between electrons and atoms.

For the correction of intensities due to the dynamical effects, the Blackman formula,[14] known as the two-beam (the incident and one diffracted beam) approximation, is commonly used in thin film

experiments by electron diffraction.[15,16,17] It is known that this theory is only applicable for crystals containing one kind of atom or else containing only light atoms, and that it is inadequate for the higher order reflections.

According to the Blackman theory, the dynamical peak intensity (I_{dyn}), corresponding to I_{kin} in eq. (4), is given by

$$I_{dyn} = I_{kin}(1/A)\int_0^A J_0(2x)\,dx \qquad (6)$$

$$A = (2\pi m_e/h^2)\cdot|F_{hkl}|\cdot D\lambda$$

, where $J_0(2x)$ is the zero order Bessel function, $|F_{hkl}|$ is the kinematical structure factor given in eq. (5), D is the thickness of crystals (or the diameter of a cluster), and λ is the electron wave length (in the present case, $\lambda = 0.061$ Å).

Plots of $\ln(I_{obs}/I_{dyn})$ vs. s^2 were carried out with varying the size parameter D systematically, since eq. (6) depends on D; typical plots for Plate A are shown in Fig. 3, denoted as (1) — (4). The deviation of the low angle reflections from a straight line, observed in the previous kinematical analysis, was completely corrected in the case of $D \simeq 80 \pm 5$ Å with the use of partial wave elastic scattering factors[18] for f in eq. (5). The size parameter thus obtained is in excellant agreement with 82 ± 10 Å, estimated from the line widths (see the previous section). A similar analysis using the Born atomic scattering factors[18] provided also a straight line, but led to a too small value in D of 60 ± 5 Å (see (3) in Fig. 3), indicating the importance of correction for intra-atomic multiple scattering effects, which are taken into account in the partial wave scattering factors.

As stated earlier, the 2nd order reflections, (400) and (440) except (222), can not be explained by the two-beam approximation; see Fig.3. The 3rd order reflections (333) and (600), which coincide with the first order (511) and (442) reflections, respectively, were also too weak. In Fig. 3, the 3rd order reflections were ignored; when they are included, all points for (511) and (442) in the Figure should be shifted downward by 0.29 and 0.22, respectively.

Parallel analyses for Plates B and C were carried out using the partial wave atomic form factor.[18] Plots of $\ln(I_{obs}/I_{kin})$ and $\ln(I_{obs}/I_{dyn})$ showed a behavior similar to the case of Plate A. The best straight lines were obtained with $D = 60 \pm 5$ Å for Plate B and $D = 50 \pm 5$ Å for Plate C, respectively, which are also consistent with those obtained from the line-width analysis. These plots are shown in Fig. 4, compared with Plate A ($D = 80$ Å); the 3rd order reflections are not included.

The slopes, $\bar{u}^2$, of these plots were determined to be 0.015 Å (Plate A), 0.017 Å^2 (B) and 0.012 Å^2 (C). Within the framework of kinematical theory for lattice vibration effects, $\bar{u}^2$ can be interpreted as mean (isotropic) square displacements of atoms, and related to the Debye characteristic temperature Θ and the sample temperature T, being approximated by ($\Theta \lesssim T$);[13,19]

$$\bar{u}^2 = 3h^2T/4\pi^2Mk\Theta^2 \qquad (7)$$

,where h is the Planck constant, M is the atomic mass of Pb, and k is the Boltzmann constant. The Debye temperature for bulk Pb crystal in the literature ranges from 68 to 105°K,[20] and for the surface atoms it has been reported to be 55 ± 10°K.[21] By allowing a range of $\Theta = 55 - 105$°K, eq. (7) gave a rough estimate of the cluster tem-

perature: T(Plate A) = 150 ± 87°K, T(B) = 170 ± 98°K, and T(C) = 120 ± 70°K.

Although the observed (first order) Bragg reflections are well explained by the use of the effective atomic scattering factor based on the two-beam approximation and the kinematical Debye-Waller factor, a close examination of scattered experimental points in Fig. 4 shows systematic fluctuations along the straight lines. The amplitude of the periodic fluctuations is enhanced as the size of clusters becomes small; in the case of the largest size (Plate A, D = 80 Å), such fluctuations die down into the experimental random noise. This fact implies that the origin of the fluctuations should arise from size effects, i.e., the nature of cluster structure, instead of other possible sources such as multiple scattering effects. The observed fluctuations of Bragg intensities are analyzed in the following section using a liquid model, and further discussed in a later section.

III) Liquid Model

In order to see the fluctuations clearly, the following function was defined;

$$R(s) = I_{obs}/I_{Bragg} \qquad (8)$$

, where $I_{Bragg} = I_{dyn} \cdot e^{-2M}$ with the notations used previously. R(s) for Plate C, in which the most marked fluctuations were observed, is plotted in Fig.5; the period of R(s) is about $s \simeq 2$ Å^{-1}. This slowly varying function of s suggests a superposition of a typical diffuse scattering as observed in a liquid or gas target.

When the Bragg intensity is superimposed on the diffuse scattering intensity I_D, due to the disordered atomic configurations, the

R(s) in eq. (8) can be equated by ,

$$R(s) = 1 + kI_D/I_{Bragg} \qquad (9)$$

,where k is a measure of the "disorderness", but its physical meaning is not clear because of the simplicity of model used here; in the following analysis k is regarded merely as a normalization constant. I_D is the Fourier transform of the atomic pair correlation function h(r),

$$I_D = f^2 n \int h(r) \exp(i\vec{r}\cdot\vec{s}) d\vec{r} \equiv f^2 n H(s) \qquad (10)$$

,where f is the effective atomic scattering factor for Pb used in the calculation of I_{Bragg}, and n is a mean number density. H(s) can be expressed by the direct correlation function C(s) in momentum space, after performing the Fourier transformation of the Ornstein-Zernike direct correlation function c(r);[22]

$$H(s) = C(s)/[1 - nC(s)], \qquad (11)$$

$$C(s) = \int c(r) \exp(i\vec{r}\cdot\vec{s}) d\vec{r}.$$

In order to evaluate eq. (11), a simple "liquid model" with particles interacting through the hard-sphere potential was employed; for most metal liquids such a model has been successfully applied to explain the liquid structure factor.[23] According to Wertheim[24] and Thiele,[25] the direct correlation function c(r) for the hard-sphere potential (sphere diameter σ) is given within the Percus-Yevick approximation[26] by a polynominal.

$$
\left.
\begin{aligned}
-c(r) &= \alpha + \beta(r/\sigma) + \gamma(r/\sigma)^3 \\
\alpha &= (1 + 2\eta)^2/(1 - \eta)^4 \\
\beta &= -6\eta(1 + \eta/2)^2/(1 - \eta)^4 \\
\gamma &= \eta(1 + 2\eta)^2/2(1 - \eta)^4 \\
\eta &= n\pi\sigma^3/6 \qquad \text{(packing-density parameter).}
\end{aligned}
\right\} \quad (12)
$$

This gives an analytical form to $H(s)$ in eq. (11).

$$
\left.
\begin{aligned}
nH(s) &= [1 + (24\eta/x^3)(a_1 \sin x - a_2 \cos x + a_3)]^{-1} - 1 \\
x &= \sigma s \\
a_1 &= \alpha + 2\beta + 4\gamma - 24\gamma/x^2 \\
a_2 &= (\alpha + \beta + \gamma)x - 12\gamma/x + a_3 \\
a_3 &= -2\beta/x + 24\gamma/x^3.
\end{aligned}
\right\} \quad (13)
$$

Then, R(s) becomes the following analytical equation, using eqs. (9), (10) and (13).

$$
R(s) = 1 + (ke^{2M}/d_{hkl}^2 P_{hkl})\{[1 + (24\eta/x^3)(a_1 \sin x - a_2 \cos x + a_3)]^{-1} - 1\}. \quad (14)
$$

Using $\sigma = 3.15$ Å, $2M = 0.012s^2$ and $\eta = 0.45$ (a typical value for most metal liquids),[23] eq. (14) was calculated at the Bragg reflection angles. The results, being normalized to 1.28 (observed value) at the (111) reflection, are plotted in Fig. 5, in comparison with the observed points. The observed periodicity and relative amplitudes are well reproduced. Another choice of the magnitudes in σ and η could give a better fit, but such an optimization was not performed.

DISCUSSION

The lattice parameter is the most direct information of the bulk structure of microclusters; whenever it is well defined, i.e. experimentally, the indexing of Bragg reflections is possible (as in the present case). Diffraction experiments of thin films indicate that the lattice parameter of microclusters is smaller than that of bulk materials, and decreases with decreasing cluster size.[27,28] It is quite conceivable that some surface effects are operating in the size dependence. One of the plausible explanations for the observation is a phenomenological one to use the concept of the elastic compression by the surface tension (S). By assuming a spherical cluster with a diameter (D) and the bulk modulus (k), the shrinkage (Δa) in the lattice parameter (a) is approximated by,

$$\Delta a = -4aS/3kD. \qquad (15)$$

When we apply this equation to the present case (Pb), for the estimate of the order of magnitudes, by the use of $k = 5 \times 10^{11}$ dyn/cm^2, [29] $S \simeq 500$ dyn/cm [30] and $a = 4.9505$ Å (of the bulk crystal);[31] the decreased lattice parameters for $D = 80$, 60 and 40 Å are 4.942, 4.939 and 4.934 Å, respectively, being compatible with the corresponding observed values: 4.939, 4.938 and 4.935 Å (see Table 2).

Another macroscopic explanation for the present case is due to a temperature effect. The linear thermal expansion coefficient for Pb is 27.08×10^{-6}/°C [32] for the range from -183°C to 14°C. The lattice parameters for Plates A, B and C due to this effect, using the estimated

temperatures [150°K (Plate A), 170°K (B) and 120°K (C)] and the bulk lattice parameter of 4.9505 Å (at 25°C), are 4.931, 4.933 and 4.927 Å, respectively; also being in reasonable agreement with the observed values.

In contrast with the above phenomenological explanations, an opposit effect due to the surface atoms may be predicted on the lattice parameter. According to the calculations,[33,34] the interplanar spacings adjacent to a planar free surface are larger than equivalent bulk spacings, and the degree of interplanar expansion diminishes rapidly with increasing depth below the surface. For instance, in the case of Pb, the percentage of increase in spacing normal to the surface plane between the first and second layers for (001), (110) and (111) surfaces is calculated to be 5.5, 4.1 and 1.6 %, respectively.[34] A LEED experiment for nickel (001) surfaces supports such a dilation of surfaces.[35] For microclusters, however, such a surface expansion as expected in the surface of bulk materials may not be applied, since in order to stabilize a microcluster system with a large portion of surface atoms, the cluster structure could be no longer simply a micro-replica of the bulk structure, as indeed demonstrated by model calculations,[4,5,36] where an icosahedral structure is stabilized relative to the f.c.c. structure.

Another effect on the change in lattice parameters may arise from crystal defects. Distortion around point imperfection in simple crystals has been calculated for a vacancy and for an interstitial atom; the shrinkage of the crystal volume due to a vacancy is estimated,[37] and for a f.c.c. crystal the first nearest neighbor distances around a vacancy decrease but the second nearest neighbor distances increase, and vice versa around an interstitial atom.[38]

Considering the above-mentioned structure change and/or possible crystal-defect effects, we have to regard the experimentally determined lattice parameter for microclusters, even when the indexing of Bragg reflections fits the case of the perfect crystal, as not only a convoluted quantity averaged over a size distribution, but also an "effective" quantity. The physical meaning of the lattice parameter becomes obscure. The closest approach distance (r_c), calculated from the experimental lattice parameter (a_e) (for the perfect f.c.c. crystal $r_c = a_e/2^{\frac{1}{2}}$), is ambiguous, and should no longer be a simple function of a_e. A more proper physical quantity for r_c is defined by the first peak of the radial distribution function, although so far it has not been done experimentally. Model calculations by Briant and Burton,[6,39] using the radial distribution functions, show the closest approach distance <u>increases</u> with <u>decreasing</u> cluster size: opposit to the case of the experimentally reduced r_c from the "effective" lattice parameter.

Therefore, care should be taken for an interpretation of the effective lattice parameter. It is merely a qualitative measure whether the microcluster possesses the characteristic of the bulk crystal structure. For more detailed information concerning the cluster structur we must rely on the analysis of the Bragg-peak intensity, as demonstrated in the present study and further discussed below. A more elaborate analysis would be a simulation of the whole diffraction intensity contour, using a cluster structure model based on molecular dynamics calculations, at the high cost of computation.

The observed periodic deviation of the Bragg-peak intensities from the pseudo-kinematical expression have been interpreted in terms of a partially amorphous structure of clusters. This may be justified

by considering possible vestiges of liquid cluster structure from the early stages of formation, followed by a relatively quick adiabatic cooling, and a large portion of surface atoms which may have many crystal defects (irregular atomic configurations). Futhermore, according to theoretical predictions,[6,36] clusters possess liquid-like surface regions but solid central regions. When the liquid phase is quenched, a disordered solid having a structure similar to that of liquid is produced.[36] However, other explanations might be possible for the diffuse scattering. In the present analysis, multiple scattering corrections were made by the simple two-beam approximation, and the thermal vibration effects were treated within the framework of kinematical theory. As mentioned before, for the higher order reflections the present two-beam theory was certainly insufficient. In multiple scattering situations, the temperature effects are more complicated than the kinematical factor e^{-2M}; correlation between displacements on neighboring atoms can enter into the theory. In addition, for surface layers, enhanced amplitudes of vibrations (of the order of 50% greater than in the bulk) and their anisotropic nature have been predicted in bulk materials.[40] These effects may also introduce a systematic error in the analysis. Further effects due to inherent scattering processes, such as inelastic-elastic scatterings (Kikuchi pattern), polarization, and reflection of electron waves by the inner potential of the crystal, were not considered in the present analysis. On the experimental side, a size distribution of clusters was not known. The deconvolution of the observed intensities by the size distribution function folded with the selective sampling effect[41] of electron diffraction was not carried out.

In spite of many unsolved problems, the present interpretation

seems reasonable (Ockham's razor), and lends experimental support for the theoretically predicted "liquid-like" solid (coexistence of regular lattices and random configurations) for microclusters.[36] If the present finding is inherent to a small size of clusters, we could expect such a characteristic fluctuation of Bragg intensities as shown in Fig. 5 for other systems. It is indeed found in the case of Ar clusters with 500 ~ 1000 atoms (size: 33 ~ 42 Å diameter, similar to the present case (Plate C)), studied by Farges et al.[1] They observed the anomaly in the peaks (111), (400) and (642), suggesting noncrystalline effects of Ar clusters. Using their observed peak heights and their kinematical intensities (given in their Table III), the corresponding analysis to Plate C (Fig. 5) has been made and is shown in Fig. 6; compare this with Fig. 5. A striking similarity can be observed for both "f.c.c." clusters. By use of eq. (14) with $\sigma = 3.4$ Å, $\eta = 0.45$, and $2M = 0.021 s^2$, the characteristic fluctuations observed in the Ar clusters can be well reproduced, as shown in the upper curve of Fig. 6.

ACKNOWLEDGMENTS

This study was supported by the Office of Naval Research and by the National Science Foundation through Gasdynamics Laboratory, Northwestern University. The author wishes to thank Professor J. Th. M. de Hosson for numerous discussions about this paper and solid state properties of metals. He is also indebted to Professors G. D. Stein and S. H. Bauer for stimulating his interest in this field and their valuable suggestions.

Table 1. Experimental Conditions for Pb Cluster Beams.

Plate	T_m(°C)[a]	T_a(°C)[b]	P_a(torr)[c]	L_h(cm)[d]	Exp.(sec)[e]
A	993	79	0.83	3.6	30
B	1040	150	0.67	2.8	20
C	932	103	0.55	2.8	20

a) The temperature of the tungsten filament, measured by an optical pyrometer; uncertainties of c.a. ± 100°C. The electric power required for these temperatures are 12 ~ 14 Amp and ~ 1 V.

b) The temperature of the mixing region, measured by a Chromel-Alumel thermocouple; see Fig. 1.

c) Argon carrier gas pressure in the mixing region.

d) The distance between the heater (H) and the first nozzle aperture (N_1); see Fig. 1.

e) Photographic exposure time.

Table 2. The observed lattice parameters, Bragg-peak intensities, average cluster sizes and cluster temperatures for Plates A, B and C.

hkl	Plate A		Plate B		Plate C	
	a(Å)	I_{obs} [a]	a(Å)	I_{obs} [a]	a(Å)	I_{obs} [a]
111	4.951	100	4.939	100	4.942	100
200	4.938	48	4.944	50	4.95	34
220	4.949	57	4.935	42	4.935	30
311	4.940	84	4.933	54	4.938	41
222	4.934	21	4.938	16	4.936	18
400	4.92	5.9	4.93	2.7	4.93	3.0
331	4.936	32	4.937	19	4.931	13
420	4.931	29	4.935	19	4.929	13
422	4.932	18	4.942	8.8	4.935	5.6
511,333	4.928	13	4.938	5.8	4.934	3.6
440	4.94	2.9	4.94	0.9	---	---
531	4.946	13	4.942	6.0	4.933	3.7
442,600	4.938	5.1	4.938	3.0		
620	4.943	5.1	4.937	1.3	---	---
533, 622	4.942	5.9	4.940	1.4	---	---
Av. a(Å) [b]	4.939 ± 0.017		4.938 ± 0.010		4.935 ± 0.015	
D(Å) [c]	82 ± 10		60 ± 5		40 ± 10	
T(°K) [d]	150		170		120	

a) Observed peak intensities, normalized to 100 at the (111) peak.
b) Average of all observed lattice parameters; uncertainties are 2.5 times their standard deviations.
c) Average cluster size in diameter, estimated from the line-width analysis; see text.
d) Cluster temperatures, estimated from the Debye-Waller-factor analysis; see text.

REFERENCES

1) J. Farges, B. Raoult and G. Torchet, J. Chem. Phys., 59, 3454 (1973).

2) P. P. Audit, J. Phys. (Paris), 30, 192 (1969).

3) J. Farges, J. Cryst. Growth, 31, 79 (1975).

4) M. R. Hoare and P. Pal, Nature Phys. Sci., 230, 5 (1971).

5) M. R. Hoare and P. Pal, ibid., 236, 35 (1972).

6) C. L. Briant and J. J. Burton, J. Chem. Phys., 63, 2045 (1975).

7) For example, J. J. Burton and C. L. Briant, "Nucleation II", A. C. Zettlemoyer (ed.), Marcel Decker, New York (1976).

8) A. Yokozeki and G. D. Stein, J. Appl. Phys., (to be published).

9) G. D. Stein and J. A. Armstrong, J. Chem. Phys., 58, 1999 (1973).

10) L. S. Bartell, J. Chem. Phys., 63, 3750 (1975).

11) L. S. Bartell, "Physical Method of Chemistry Techniques of Chemistry," 1, A. Weissberger (ed.), Wiley, New York (1972).

12) International Tables for X-ray Crystallography, C. H. MacGillavry and G. D. Reck (eds.), 3, 318 (1968).

13) A. H. Compton and S. K. Allison, "X-ray in Theory and Experiment", D. Van Nostrand Co. Inc., New Jersey (1935).

14) M. Blackman, Proc. Roy. Soc., A173, 68 (1939).

15) V. M. Horstmann and G. Meyer, Acta Cryst., 15, 271 (1962).

16) J. M. Cowley and S. Kuwabara, ibid., 15, 260 (1962).

17) T. B. Rymer, "Electron Diffraction", Methuen and Co. Ltd., London (1970).

18) International Tables for X-ray Crystallography, J. A. Ibers and W. C. Hamilton (eds.), 4, 248 and 162 (1974).

19) L. Catz, Proc. Phys. Soc., B68, 951 (1955).

20) Reference (12), page 234.

21) R. M. Goodman, H. H. Farrell and G. A. Somorjai, J. Chem. Phys., 48, 1046 (1968).

22) L. S. Ornstein and F. Zernike, Proc. Akad. Sci. (Amsterdam), 17, 793 (1914).

23) N. W. Ashcroft and J. Lekner, Phys. Rev., 145, 83 (1966).

24) M. S. Wertheim, Phys. Rev. Lett., 10, 321 (1963).

25) E. Thiele, J. Chem. Phys., 39, 474 (1963).

26) J. K. Percus and G. J. Yevick, Phys. Rev., 110, 1 (1958).

27) D. Schoeer, R. F. Marzke, D. J. Erickson, S. W. Marshall and R. M. Wilenzick, Phys. Rev., B2, 4414 (1970).

28) P. F. Vergand, Phil. Mag., 31, 537 (1975).

29) R. J. Stephenson,"Mechanics and Properties of Matter", page 239, John Wiley & Sons Inc., New York (1952).

30) B. C. Allen, "Liquid Metals", S. Z. Beer (ed.), page 186, Marcel Dekker Inc., New York (1972).

31) H. E. Swanson and E. Tage, NBS Circular 539, 1, 34 (1953).

32) Handbook of Chemistry and Physics, 43rd ed., page 2278, CRC Press, Ohio (1962).

33) P. A. Tick and A. F. Witt, Surface Sci., 26, 165 (1971).

34) J. J. Burton and G. Jura, J. Phys. Chem., 71, 1937 (1967).

35) S. Anderson and J. B. Pendry, J. Phys. C6, 601 (1973).

36) J. J. Burton, Cat. Rev. Sci. Eng., 9, 209 (1974).

37) H. Kanzaki, J. Phys. Chem. Solids, 2, 24 (1957).

38) G. L. Hall, ibid., 3, 210 (1957).

39) C. L. Briant and J. J. Burton, Surface Sci., 51, 345 (1975).

40) J. B. Pendry, "Low Energy Electron Diffraction", Acad. Press, London and New York (1974).

41) G. G. Libowitz and S. H. Bauer, J. Phys. Chem., 59, 214 (1955).

FIGURE CAPTIONS

Figure 1. Schematic diagram (not to scale) of the nozzle for metal cluster beams; see text.

Figure 2. Photographic density (O.D.) of the diffraction patterns of Pb clusters for Plates A, B and C, plotted as a function of the scattering variable s; Miller indices are given in A.

Figure 3. Logarithmic plots of the ratio of the observed Bragg-peak intensity I_{obs} (Plate A) to the calculated intensity I_{calc}, plotted as a function of s^2 (Debye-Waller-factor analysis). I_{calc} ($= I_{dyn}$ in eq. (6) of text) was calculated using partial wave (PW) and Born atomic scattering factors with various size parameter D; (1) $D = 90\mathring{A}$ (PW); (2) $D = 80\mathring{A}$ (PW); (3) $D = 60\mathring{A}$ (Born); (4) $D = 60\mathring{A}$ (PW); and (5) $D = 0$ (PW), equivalent to $I_{calc} = I_{kin}$ in eq. (4) of text (kinematical analysis).

Figure 4. Plots similar to Figure 3 (Debye-Waller-factor analysis) for Plates A, B and C. Only the best straight line for each Plate is shown: for A the same as (2) in Figure 3, for B $D = 60\mathring{A}$ (PW), and for C $D = 50\mathring{A}$ (PW), respectively.

Figure 5. The fluctuations R(s) of Bragg-peak intensities (Pb clusters: Plate C). The lower curve is the observed R(s), defined by eq. (8), and the upper curve is the calculated R(s) by eq. (14), based on the "liquid model" described in text. The calculated points are normalized to 1.28 (the observed value) at (111). The dotted lines are merely drawn to accentuate the characteristics of fluctuations.

Figure 6. The fluctuations R(s) of Bragg-peak intensities for Ar clusters: plots similar to Figure 6. The observed points are taken from the Table III of Ref. 1; see text. The calculated points are normarized to 1.5 (the observed value) at (111).

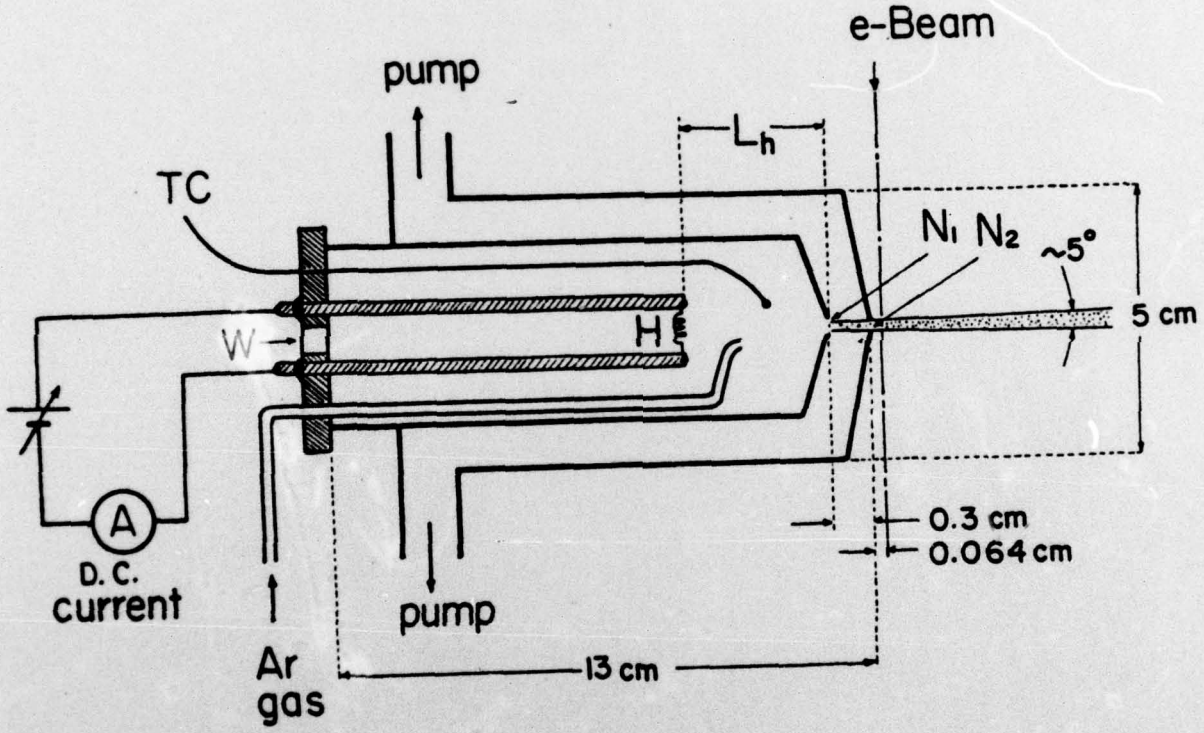
e-Beam
pump
L_h
TC
N_1 N_2
~5°
5 cm
W
H
A
D.C.
current
0.3 cm
0.064 cm
pump
Ar
gas
13 cm

Figure 1

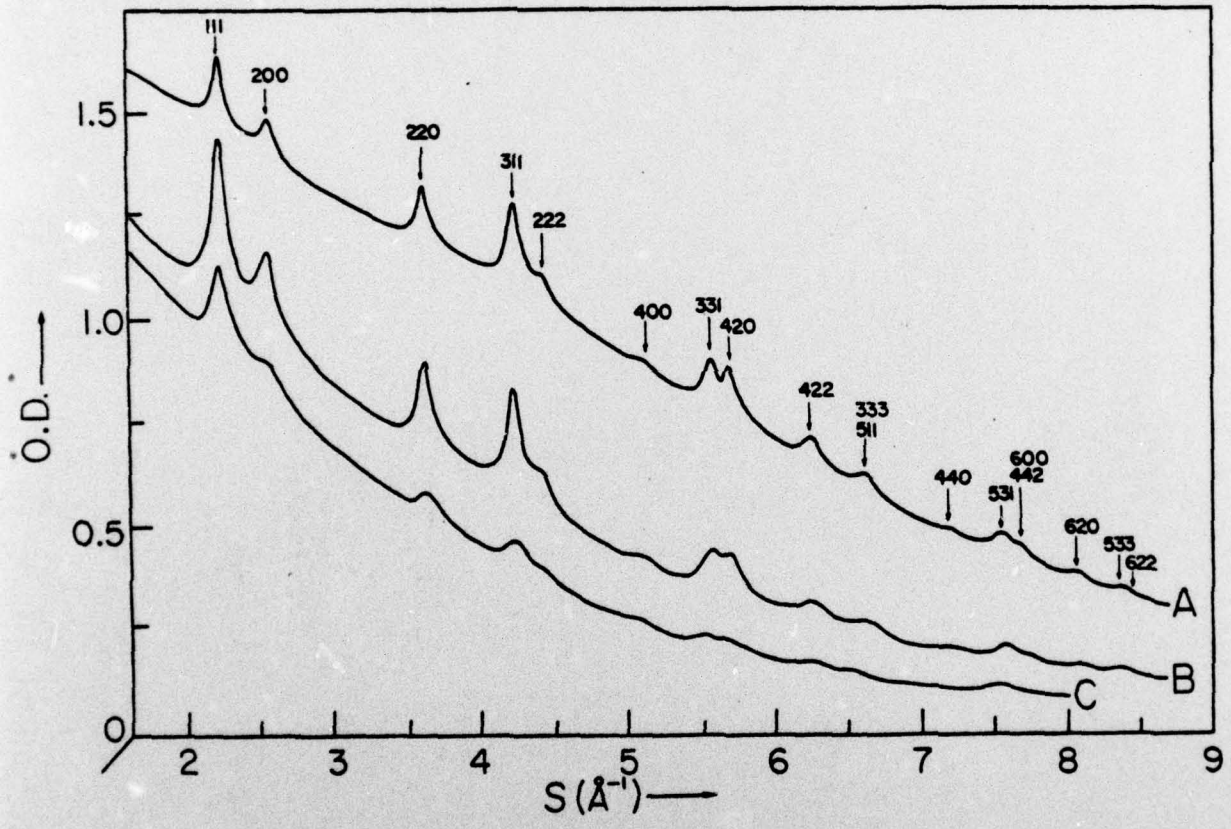
111
200
220
311
222
400
331
420
422
333
511
440
531
600
442
620
533
622
A
B
C
O.D.
S(Å⁻¹)
0
0.5
1.0
1.5
2
3
4
5
6
7
8
9

Figure 2

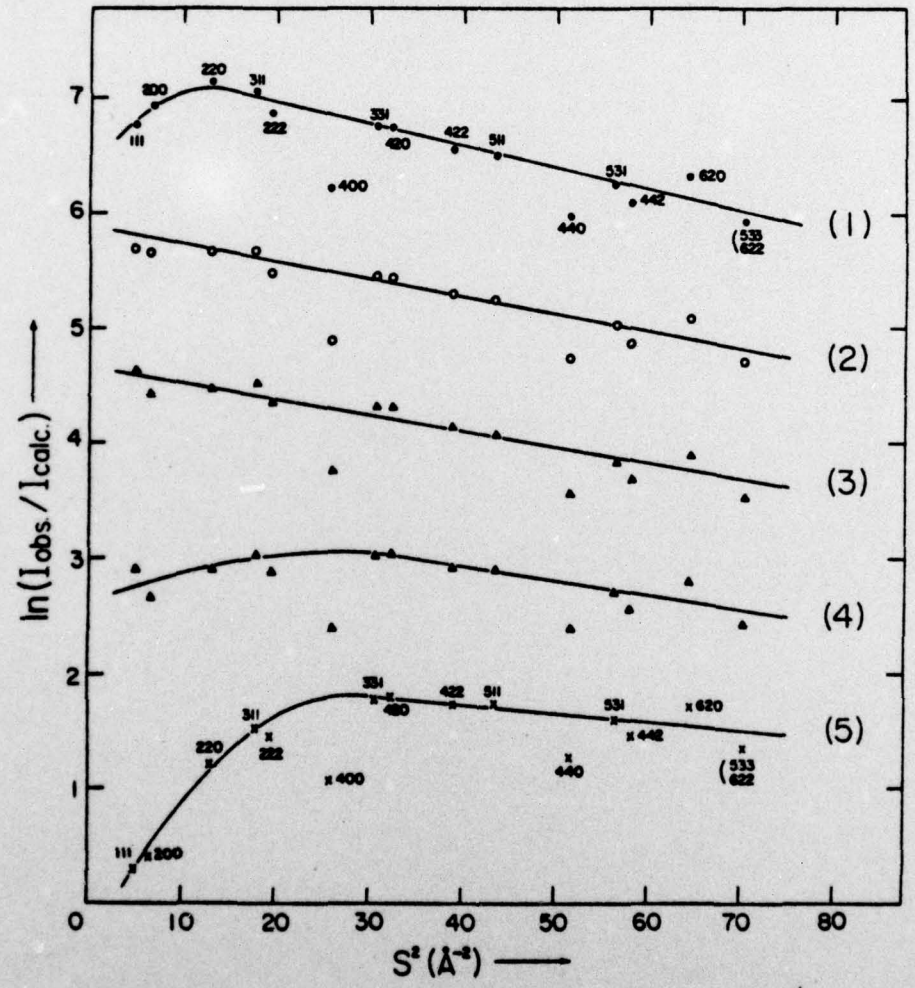
ln(Iobs./Icalc.)
S² (Å⁻²)
(1)
(2)
(3)
(4)
(5)
111
200
220
311
222
400
331
420
422
511
440
531
442
620
533
622

Figure 3

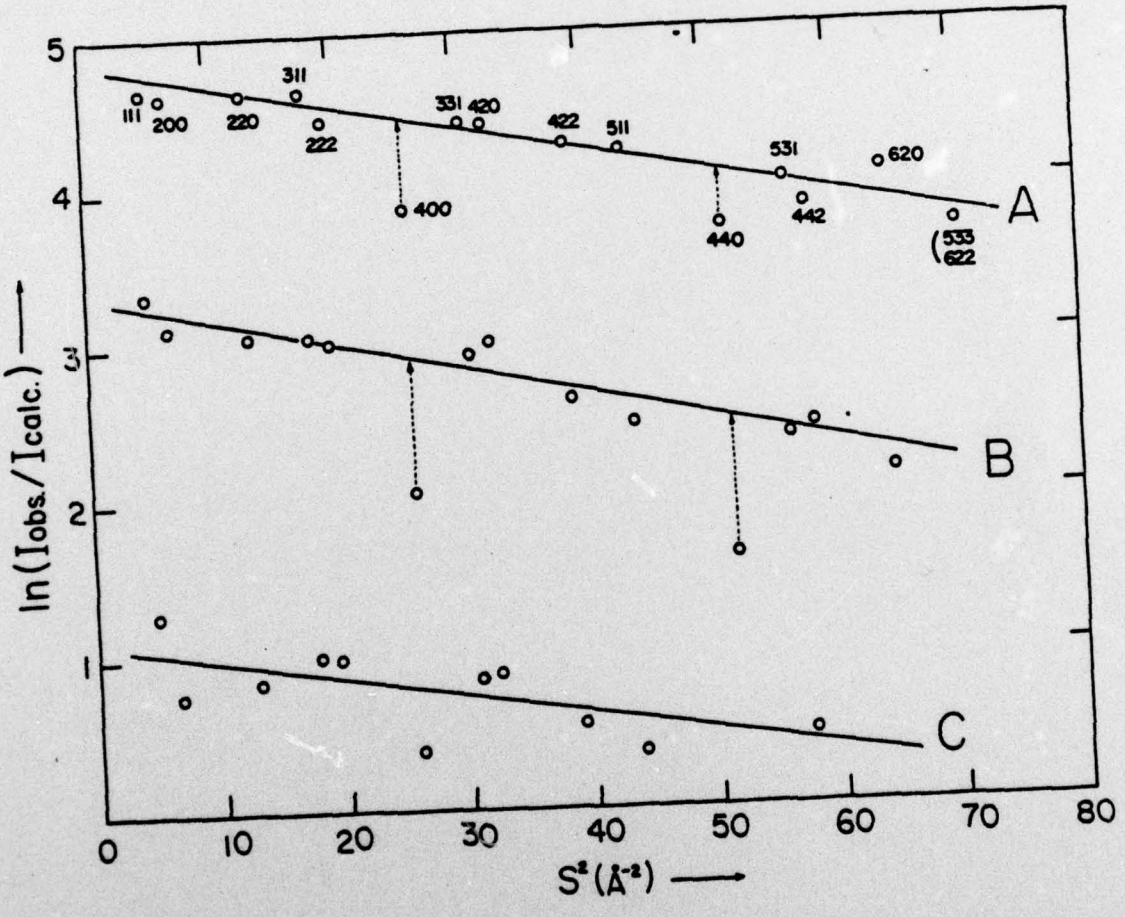
5
4
3
2
1
0
10
20
30
40
50
60
70
80
ln(Iobs/Icalc.) ⟶
S² (Å⁻²) ⟶
111
200
220
311
222
400
331
420
422
511
440
531
442
620
(533
622
A
B
C

Figure 4

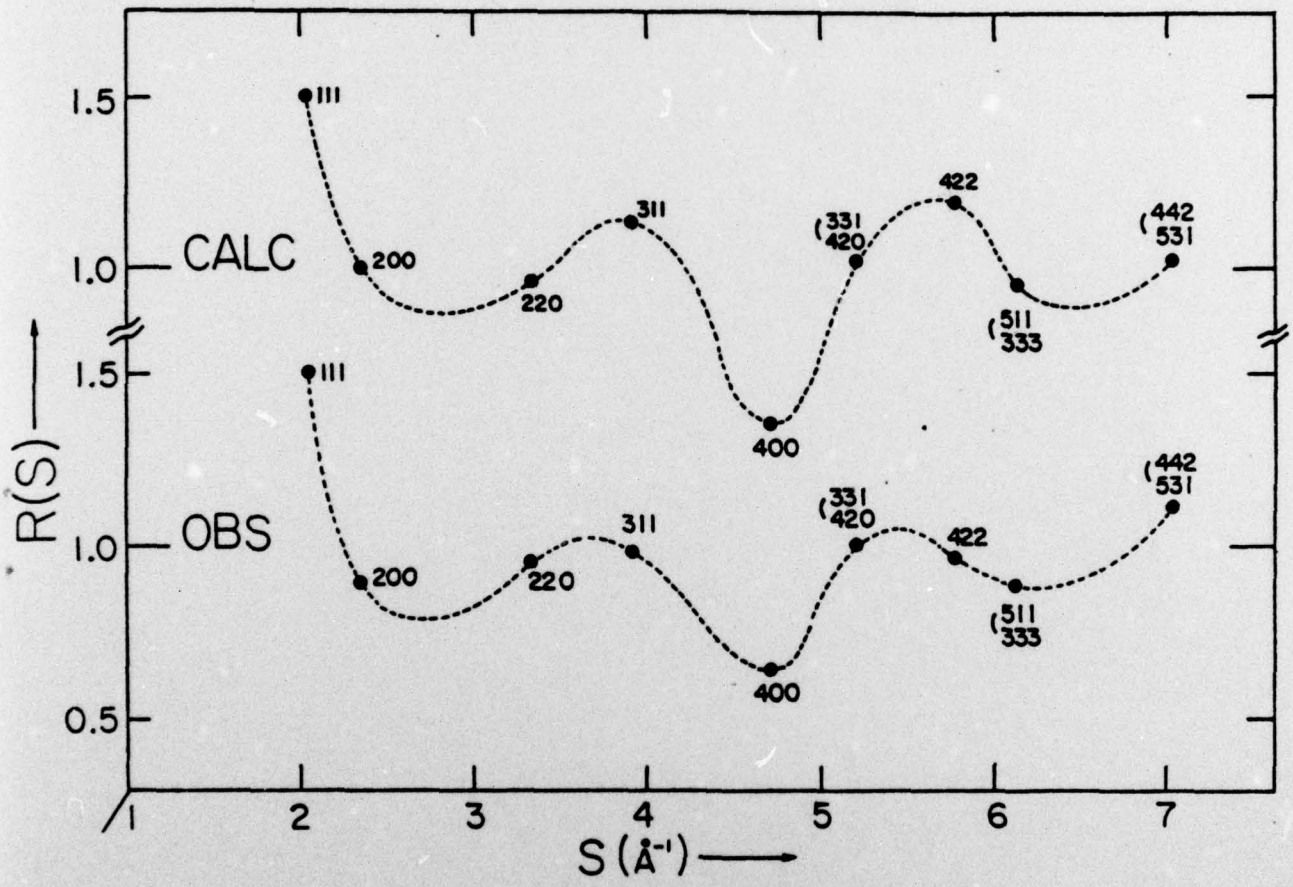
1.5
1.0
CALC
111
200
220
311
400
(331
420
422
(511
333
(442
531
1.5
1.0
OBS
0.5
R(S)
111
200
220
311
400
(331
420
422
(511
333
(442
531
1
2
3
4
5
6
7
S (Å⁻¹)

Figure 5

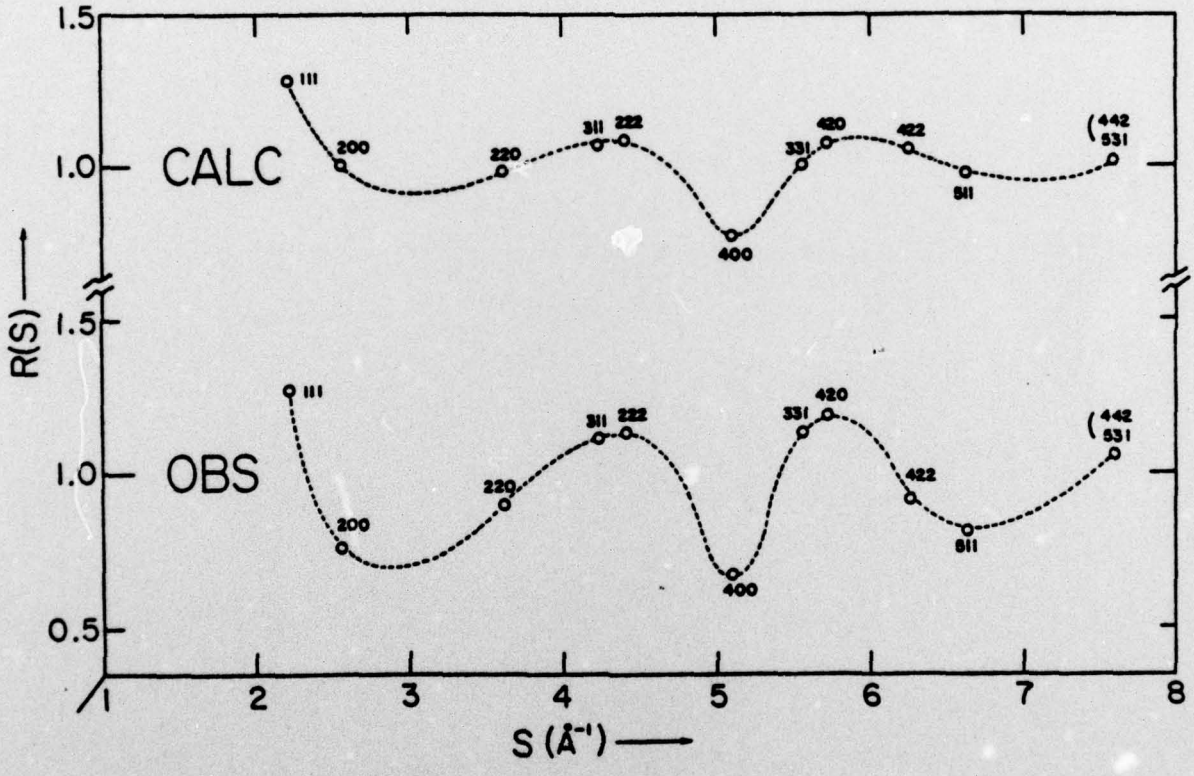
1.5
1.0
CALC
111
200
220
311
222
400
331
420
422
511
(442
531
1.5
1.0
0.5
OBS
111
200
220
311
222
400
331
420
422
511
(442
531
R(S)
1
2
3
4
5
6
7
8
S (Å⁻¹)

Figure 6